Naval Research Laboratory

Washington, DC 20375-5320

NRL/MR/7322--19-9954

Rogue Wave Events in Time Series of Surface Elevation

MarkD. Orzech
David W. Wang

Ocean Dynamics & Prediction Branch
Oceanography Division

November 13, 2019

REPORT DOCUMENTATION PAGE

Form Approved
OMB No. 0704-0188

1. REPORT DATE *(DD-MM-YYYY)*	**2. REPORT TYPE**	**3. DATES COVERED** *(From - To)*
13-11-2019	NRL Memorandum Report	01 Jan 2017 – 25 Sept 2019

4. TITLE AND SUBTITLE

Rogue Wave Events in Time Series of Surface Elevation

5a. CONTRACT NUMBER

5b. GRANT NUMBER

5c. PROGRAM ELEMENT NUMBER

6. AUTHOR(S)

Mark D. Orzech and David W. Wang

5d. PROJECT NUMBER

5e. TASK NUMBER

5f. WORK UNIT NUMBER
6A51

7. PERFORMING ORGANIZATION NAME(S) AND ADDRESS(ES)

Naval Research Laboratory
1009 Balch Blvd
Stennis Space Center, MS 39529-5004

8. PERFORMING ORGANIZATION REPORT NUMBER

NRL/MR/7322--19-9954

9. SPONSORING / MONITORING AGENCY NAME(S) AND ADDRESS(ES)

Office of Naval Research
One Liberty Center
875 N. Randolph Street, Suite 1425
Arlington, VA 22203-1995

10. SPONSOR / MONITOR'S ACRONYM(S)

ONR

11. SPONSOR / MONITOR'S REPORT NUMBER(S)

12. DISTRIBUTION / AVAILABILITY STATEMENT

DISTRIBUTION STATEMENT A: Approve for public release; distribution is unlimited.

13. SUPPLEMENTARY NOTES

14. ABSTRACT

This report describes a comprehensive analysis of roughly two decades of surface elevation time series from Datawell wave buoys maintained by CDIP at UC San Diego. Hourly sections of the time series are examined to identify rogue wave events, recording wave sizes, times of occurrence, and geographic locations. The initial dataset is subjected to a quality control process to eliminate identifiable "false positives". A preliminary analysis is performed at several buoy locations to investigate the correlation of rogue events with cotemporal data on ocean currents. Statistics of the roughly 8500 identified rogue events are summarized, and results of the preliminary wave-current analysis are presented. Planned future work is described.

15. SUBJECT TERMS

Rogue waves
Surface elevation time series
Buoy data
Wave-current interaction

16. SECURITY CLASSIFICATION OF:			**17. LIMITATION OF ABSTRACT**	**18. NUMBER OF PAGES**	**19a. NAME OF RESPONSIBLE PERSON**
a. REPORT	**b. ABSTRACT**	**c. THIS PAGE**			Mark D. Orzech
Unclassified Unlimited	Unclassified Unlimited	Unclassified Unlimited	Unclassified Unlimited	21	**19b. TELEPHONE NUMBER** *(include area code)* (228) 688-5974

Standard Form 298 (Rev. 8-98)
Prescribed by ANSI Std. Z39.18

This page intentionally left blank.

Contents

1 INTRODUCTION 3
2 DESCRIPTION OF DATASETS 4
2.1 Wave data 4
2.2 Ocean current data 6
3 ANALYSIS METHODS 6
3.1 Wave time series and spectra 6
3.2 Preliminary wave-current analysis 6
4 RESULTS 7
4.1 Rogue wave event statistics 7
4.2 Results of preliminary current analysis 10
5 CONCLUSIONS AND FUTURE WORK 17
6 REFERENCES 19

List of Figures

Figure 1. Locations of analyzed buoys (NB: Only selected analysis results – from buoy #029 – are included in this report). 10
Figure 2. ***Current-only*** analysis results from analysis of rogue wave event at CDIP buoy #29, 08 Feb 2002. Panels show: (a) Original surface elevation time series from buoy. (b) Close up view of 8.7m rogue wave (solid blue line) selected from time series (dashed blue). (c) Scatter plot of wave period (T) vs. normalized wave height (H/H_s) for all waves in the one-hour selection. (d) Wave frequency spectrum (black line), ocean current nautical ("from") direction (θ_c, blue dashed line), and wave Cartesian ("to") direction (θ_w, red circles), plotted versus wave frequency. (*NB: Y-axis on this panel gives units of both **10*[spectral density]** and directional **degrees rel true N***.) Currents are directly opposing the waves for most of the frequencies surrounding the spectral peak. 11
Figure 3. ***Current gradient*** analysis results for rogue event identified at buoy #029, 24 Feb 2008. Format is same as that of Figure 2, except that lower right panel also includes a green dashed line representing the Cartesian ("to") direction computed for the surface current gradient. For the event shown, the wave direction at the spectral peak frequency $\theta_w(f) \approx 170°$, while the current gradient direction $\theta_g \approx 10°$, so that $|\theta_w(f) - \theta_g| \approx 160°$, indicating that the peak waves are propagating into a primarily negative current gradient in this case. 12
Figure 4. Current gradient analysis results for rogue event identified at buoy #029, 06 Mar 2008. Format is same as that of Figure 3. For the event shown, the wave direction at the spectral peak frequency $\theta_w(f) \approx 300°$, while the current gradient direction $\theta_g \approx 60°$, so that $|\theta_w(f) - \theta_g| \approx 140°$, indicating that the peak waves are again propagating into a primarily negative current gradient in this case. 13
Figure 5. Current gradient analysis results for rogue event identified at buoy #029, 21 Mar 2008. Format is same as that of Figure 3. For the event shown, the wave direction at the spectral peak frequency $\theta_w(f) \approx 300°$, while the current gradient direction $\theta_g \approx 190°$, so that $|\theta_w(f) - \theta_g| \approx 110°$, indicating that the peak waves are propagating into an only weakly negative current gradient in this case. 14
Figure 6. Current gradient analysis results for rogue event identified at buoy #029, 15 Mar 2008. Format is same as that of Figure 3. For the event shown, the wave direction at the spectral peak frequency $\theta_w(f) \approx 260°$, while the current gradient direction $\theta_g \approx 310°$, so that $|\theta_w(f) - \theta_g| \approx 50°$, indicating that the peak waves are propagating into a positive current gradient in this case, contrary to what would be expected for most current-forced rogue wave events. 15
Figure 7. Current gradient analysis results for rogue event identified at buoy #029, 09 Dec 2004. Format is same as that of Figure 3. For the event shown, the wave direction at the spectral peak frequency $\theta_w(f) \approx 300°$, while the current gradient direction $\theta_g \approx 260°$, so that $|\theta_w(f) - \theta_g| \approx 40°$, indicating (as in Figure 6) that the peak waves are propagating into a positive current gradient, contrary to what would be expected for most current-forced rogue wave events. 16
Figure 8. Location of buoys #029 (top) and #071 (bottom) over bathymetry. Buoy is near shelf edge in each case. 17

List of Tables

Table 1. Details of CDIP buoys from which surface elevation time series data were acquired. Fifth column ("Dates") provides range of dates (MM/YY) processed for each buoy ("pres." = present day, currently 12/2018, but will be extended in future analyses). Sixth column ("Location") describes landmark nearest the buoy location (CA = California, HI = Hawaii, OR = Oregon, FL = Florida, NH = New Hampshire, Oc Stn Papa = Ocean Station Papa in Gulf of Alaska). Lines in ***bold italics*** are buoys whose depth is less than 150m. 5
Table 2. Summary of rogue wave events identified at 34 CDIP Datawell buoys. Columns 4-6 display total rogue waves with height exceeding 1m, 6m, and 10m, respectively, as counted over entire measurement period at each location. 9

1 INTRODUCTION

Ocean surface waves that are anomalously large relative to other waves in their local environment are often designated as "rogue waves". They are most commonly defined as waves whose height, H_r, is greater than twice the local significant wave height, H_s (i.e., the average height of the largest third of the waves in a given area); i.e., $H_r > 2*H_s$. An alternative definition relates the crest elevation above mean sea level, η_r, to H_s: $\eta_r > 1.25*H_s$. Thus, while a 2m rogue wave in 1m seas will not scare many ship captains, an unexpected 20m rogue wave in 10m seas could cause considerable damage, injury, and even death on many vessels.

As implied by their name, rogue waves are relatively rare. Nevertheless, it is generally accepted among ocean scientists that large rogues do occur, and a considerable amount of research has been done in an attempt to explain their physical origins and identify the primary environmental factors that cause them to develop.

Research into environmental factors contributing to rogue wave development suggests that ocean currents, wind forcing, and wave directional distribution can play a role in either accelerating or dampening the growth of extreme waves. Onorato et al. (2011), Manolidis et al. (2019) and others suggest that current gradients that oppose the wave direction, with current magnitude increasing as the waves propagate farther, can modulate the wave spectrum and increase the Benjamin Feir Index (BFI; Janssen, 2003), a common measure of rogue wave likelihood. Babanin & Rogers (2014) suggest that strong wind forcing in the direction of wave propagation can act as a limiter on rogue wave growth by augmenting high-frequency components of the wave spectrum and thereby fomenting wave breaking. Onorato et al. (2009) and Waseda et al. (2009) showed that frequency modulation in typical wave spectra is inversely correlated with their directional spread, so that steep waves in directionally narrow spectra will experience more nonlinear frequency modulation. While we do not address most of these causal factors in the report below, we do conduct a limited investigation of horizontal ocean current gradients coincident with several identified rogue wave events.

This report documents a comprehensive analysis of ocean surface wave buoy time series, which produced an extensive dataset of 8499 confirmed rogue wave events. The analysis relied on data from 34 Datawell Waverider buoys maintained by the Coastal Data Information Program (CDIP), Integrative Oceanography Division, operated by the Scripps Institution of Oceanography under the sponsorship of the U.S. Army Corps of Engineers and the California Department of Parks and Recreation.

Dataset ranges, formats, access, and basic processing are described in Section 2. The procedures for identification and quality control (QC) of rogue wave events and the selection of cotemporal wind and current data are detailed in Section 3. Section 4 presents statistical results from the rogue wave analysis and from a preliminary examination of ocean current data during rogue events at a selected "hot-spot" buoy. Conclusions and descriptions of upcoming work are provided in Section 5.

Manuscript approved September 26, 2019.

2 DESCRIPTION OF DATASETS

This investigation primarily made use of datasets for waves, but model data for ocean currents and 10m winds were also utilized as part of an exploratory secondary analysis. As mentioned above, the wave data, including both spectra and time series, were obtained from Datawell Waverider buoys (Datawell BV, 2009) maintained by CDIP. Ocean current fields were obtained from the NCEP Climate Forecast System, version 2 (reanalysis, 2011-present[1]). More details on each dataset are provided below.

2.1 Wave data

Wave data were obtained in netCDF format from the THREDDS server on the CDIP website (http://thredds.cdip.ucsd.edu/thredds/catalog/cdip/archive/catalog.html). Table 1 provides information about the 34 Datawell buoys from which data were obtained, including buoy numbers, locations, and date-time ranges processed.

Over half the buoys are located off the coast of California, while about one fifth are near Hawaii. Only two buoys are in the Atlantic Ocean (New Hampshire and Florida), while four are near islands in the western Pacific (Guam, Marshall Islands, Saipan). By far the deepest measurement location is Ocean Station Papa, at 4252m depth in the Gulf of Alaska. There are 29 stations in water depth greater than 150m, of which 19 are deeper than 300m, 11 are deeper than 500m, and four are deeper than 1000m.

Lengths of processed time series range from 2.6 years at the Marshall Islands buoy (#163) to 23 years at the Point Reyes, CA buoy (#029). The total length of the combined time series is nearly 400 years (see Table 2). Most time series are reasonably continuous, although many have at least short periods (i.e., days – months) without data. For specific details on the deployment times of each buoy, visit the main CDIP website (http://cdip.ucsd.edu) and search for the buoy number.

[1] Version 1 (1979-2010) will also be utilized in the near future, as part of a comprehensive validation of a rogue threat estimation system (see Section 5).

Table 1. Details of CDIP buoys from which surface elevation time series data were acquired. Fifth column ("Dates") provides range of dates (MM/YY) processed for each buoy ("pres." = present day, currently 12/2018, but will be extended in future analyses). Sixth column ("Location") describes landmark nearest the buoy location (CA = California, HI = Hawaii, OR = Oregon, FL = Florida, NH = New Hampshire, Oc Stn Papa = Ocean Station Papa in Gulf of Alaska). Lines in ***bold italics*** are buoys whose depth is less than 150m.

Buoy #	Lon (deg W)	Lat (deg N)	Depth (m)	Dates	# Years	Location
028	118.63	33.85	363	4/00 – pres.	18.5	CA
029	123.47	37.95	550	12/96 – pres.	23	CA
067	119.88	33.22	335	1/00 – pres.	19	CA
071	120.78	34.45	549	3/98 – pres.	20.8	CA
091	117.44	32.63	186	12/95 – 8/05	9.7	CA
092	118.32	33.62	457	3/98 – pres.	20.8	CA
093	117.37	32.75	192	11/97 – 12/15	18.2	CA
094	124.73	40.29	319	4/99 – pres.	19.6	CA
100	117.39	32.93	550	2/01 – pres.	17.9	CA
107	119.80	34.33	183	7/02 – 8/16	14.1	CA
111	***119.43***	***34.17***	***113***	***7/02 – pres.***	***16.4***	***CA***
156	121.95	36.76	168	6/07 – 5/16	9	CA
157	122.10	36.34	366	11/08 – pres.	11.1	CA
185	122.35	36.72	1463	10/11 – pres.	7.2	CA
191	117.42	32.53	1143	10/07 – pres.	11.2	CA
203	119.55	33.76	1910	7/13 – pres.	5.5	CA
216	120.77	34.44	576	7/15 – pres.	3.5	CA
222	121.50	34.77	647	3/16 – pres.	2.8	CA
098	***157.68***	***21.41***	***89***	***8/00 – pres.***	***18.3***	***HI***
106	158.12	21.67	200	1/02 – pres.	17	HI
165	158.12	21.28	300	11/10 – 12/17	7.1	HI
187	156.43	21.02	193	12/11 – pres.	7.1	HI
188	154.97	19.78	350	3/12 – pres.	6.8	HI
198	***157.75***	***21.48***	***81***	***11/12 – pres.***	***6.2***	***HI***
202	159.57	22.28	200	10/13 – pres.	5.3	HI
139	124.55	43.77	183	8/06 – pres.	12.3	OR
179	124.64	46.13	183	4/11 – pres.	7.7	OR
144	***84.27***	***27.34***	***94***	***7/07 – pres.***	***11.4***	***FL***
160	***70.17***	***42.80***	***76***	***9/08 – pres.***	***11.2***	***NH***
121	-144.79	13.35	200	8/03 – pres.	15.3	Guam
196	-144.81	13.68	515	11/12 – pres.	6.2	Guam
163	-171.39	7.08	540	5/16 – pres.	2.6	Marshall Isl.
166	145.20	50.03	4252	7/10 – pres.	8.4	Oc Stn Papa
197	-145.66	15.27	490	11/12 – pres.	6.2	Saipan

2.2 Ocean current data

As noted earlier, ocean surface current fields were obtained from the NCEP CFSv2 reanalysis for selected time periods (Saha et al., 2010). The Climate Forecast System (CFS) is a run by the National Centers for Environmental Prediction (NCEP) that encompasses both weather and climate timescales. Version 2 (CFSv2), which is run once daily, became operational in 2011. It overlaps to some degree with U.S. government models at shorter timescales, such as the Global Forecast System and NAVGEM. CFS couples atmospheric to oceanic modeling, deriving its forecasts from a 16-member ensemble. The downloaded data included hourly averaged U (i.e., positive eastward) and V (positive northward) current components for the uppermost 5m of water depth.

3 ANALYSIS METHODS

In this section, we describe the methods by which the datasets described above were analyzed, beginning with the processing and quality control of wave time series to select and validate rogue wave events. Following this, we describe a limited qualitative examination we conducted of the current and wind conditions at times and locations of rogue wave events at several buoys.

3.1 Wave time series and spectra

Available data (for periods of 1-20 years) from each of 34 buoys were processed with a python-based script that analyzed periods of one hour at a time. For each hour of data, the software used a zero-upcrossing method to identify and measure each wave, determining significant wave height H_s by averaging the heights of the 1/3 largest waves in the hour-long time series. Any waves with height $H > 2.0H_s$ were identified, and their locations, timestamps, and magnitudes were saved.

A quality control procedure was applied to the identified rogue waves to eliminate false positives caused by electrical or other noise-related malfunctions, anomalous or resonant buoy motion, etc. The QC procedure included the following rules for each hourly time series:

- Kurtosis, κ: Low-pass, accepting only cases with $\mathbf{2 < \kappa < 6}$
- Wave crest elevation, η_c: Restrict to $\boldsymbol{\eta_c < 1.5 \cdot H_s}$
- Horizontal buoy excursion, Δx, Δy: Limit measured values to $\boldsymbol{\Delta x < 1.8 \cdot H_{s,x}}$, $\boldsymbol{\Delta y < 1.8 \cdot H_{s,y}}$ (where $H_{s,i} = 4 \cdot \sigma_i$ = four times standard deviation of buoy time series in x- or y-direction)
- Significant wave height, H_s: Require $\boldsymbol{H_s > 1\text{m}}$ for vertical (z-direction) time series

For events that met these criteria, the hour-long time series was saved to a file, and statistics (including rogue height(s), number of rogues identified, and H_s) were appended to a data table of results for the specific buoy. Cases with multiple rogues or extreme rogues ($\eta_c > 1.4 \cdot H_s$) were specially marked, to facilitate future manual examination of the time series.

3.2 Preliminary wave-current analysis

Combining identified rogue wave events with the corresponding buoy measured frequency directional spectra and CFSv2-modeled ocean surface currents, we conducted preliminary tests

of the results of Manolidis et al. (2019) and others described in the Introduction. According to those publications, waves that propagate against (or with) a surface current that is decelerating will experience a nonlinear transfer of energy that can increase the modulational instability of the wave spectrum and make rogue wave development more likely.

In this analysis, we extracted time series and wave spectra from several buoys for periods when rogue waves were detected. We also obtained CFSv2 surface current estimates in the vicinity of each buoy for each identified rogue period. The gradient of the current at WW3 grid location (*i, j*) and its modulating effect on a given wave of frequency *f* are calculated as follows:

1. Current gradients in *x*-dir: $$\partial U_{i,j} / \partial x = \left(U_{i+1,j} - U_{i-1,j}\right) / 2 \cdot dx$$
2. Current gradients in *y*-dir: $$\partial V_{i,j} / \partial y = \left(V_{i,j+1} - V_{i,j-1}\right) / 2 \cdot dy$$
3. Magnitude of gradient at *(i, j)*: $$\Delta U_{i,j} = \sqrt{\left(\partial U_{i,j} / \partial x\right)^2 + \left(\partial V_{i,j} / \partial y\right)^2} \cdot \sqrt{dx^2 + dy^2}$$
4. Angle of gradient at *(i, j)*: $$\theta_g = tan^{-1}\left(\frac{\partial V_{i,j} / \partial y}{\partial U_{i,j} / \partial x}\right)$$

From this, we then determine the modulating effect on waves at *(i, j)* as follows:

$$Q_{mod}(f) = \Delta U_{i,j} * cos\left(\theta_w(f) - \theta_g\right) \quad (1)$$

where $\theta_w(f)$ = wave direction at each frequency *f* (values of θ_w provided with buoy spectra from CDIP). The earlier cited theoretical and modeling work suggests that the value of $Q_{mod}(f)$ for identified rogue wave events should be larger and negative, particularly for frequencies *f* that are close to the spectral peak frequency.

In Section 4.2, we present sample results determined using this procedure for rogue wave events at several buoys, comparing wave spectra values and directions θ_w at all frequencies *f* to the current gradient angle θ_g at the buoy location for selected times.

4 RESULTS

This section summarizes the characteristics of the rogue wave events identified using the selection and QC methods that were described in Section 3.1, and then presents initial results of the preliminary wave-current analysis that was described in Section 3.2.

4.1 Rogue wave event statistics

Following the analysis described in Section 3.1, a total of 8499 rogue wave events with rogue height H_r > 1m were identified. Of these, 808 involved waves with height H_r > 6m and 76 involved waves with H_r > 10m. More detailed results are presented below in Table 2.

The largest total number of rogue events (756) was detected at buoy #071, located off the California coast near Santa Barbara. This corresponded to approximately 36 rogue events per year at that site. The highest rate of rogue wave occurrence at any of the measured locations was 47 per year at #163 near the Marshall Islands, which has only been active since mid-2016. In the

category of extreme rogue events (H_r > 10m), the largest tally was 22, recorded over roughly 7 years at buoy #166, Ocean Station Papa in the Gulf of Alaska. Such extreme waves were detected at 11 of the 34 buoy locations during the periods analyzed. The largest rogue wave, with H_r = 24.14m, was also measured at Ocean Station Papa. Other extreme heights that were measured included a 16.3m wave at buoy #139, an 18.0m wave at buoy #160, and 12-13m waves at #071 and #094.

For QC'ed results, the ratio of rogue wave height to significant wave height (i.e., H_r / H_s) in the dataset ranged from 2.0 to 2.5 for rogues greater than 6m. Extreme waves with H_r > 10m and $H_r \geq 2.4 \cdot H_s$ were recorded at buoys #029, 094, 139, and 160, and similarly large waves with $H_r \geq 2.3 \cdot H_s$ were measured at #067, 157, and 166.

Potentially the most dangerous rogue wave in this dataset, recorded at Ocean Station Papa, was the 24m wave noted above, which reached 2.34 times the local significant wave height. A vessel relying only on forecasts of H_s from WAVEWATCH III® (WW3DG, 2019) would have been expecting waves of "only" 10-11m at the time and location where this anomalous giant was measured. For reference, the flight deck of a typical U.S. Navy aircraft carrier has a freeboard of roughly 18m above the water surface. Large container ships have a freeboard of 12-15m when fully loaded. While the predicted waves would thus be of only moderate concern to either vessel type, the measured rogue wave would have easily swamped both ships' main decks and potentially even damaged the higher parts of their superstructures.

Table 2. Summary of rogue wave events identified at 34 CDIP Datawell buoys. Columns 4-6 display total rogue waves with height exceeding 1m, 6m, and 10m, respectively, as counted over entire measurement period at each location.

Buoy #	# Years	Location	Number of Rogue Events		
			H_r > 1m	H_r > 6m	H_r > 10m
028	18.5	CA	214	0	0
029	23	CA	707	150	8
067	19	CA	596	50	2
071	20.8	CA	756	92	4
091	9.7	CA	81	0	0
092	20.8	CA	218	5	0
093	18.2	CA	157	2	0
094	19.6	CA	552	147	16
100	17.9	CA	164	2	0
107	14.1	CA	201	1	0
111	***16.4***	***CA***	***238***	***0***	***0***
156	9	CA	235	7	0
157	11.1	CA	212	29	5
185	7.2	CA	112	12	0
191	11.2	CA	159	0	0
203	5.5	CA	24	0	0
216	3.5	CA	90	14	1
222	2.8	CA	79	14	1
098	***18.3***	***HI***	***602***	***12***	***0***
106	17	HI	554	21	1
165	7.1	HI	112	0	0
187	7.1	HI	85	6	0
188	6.8	HI	148	15	0
198	***6.2***	***HI***	***91***	***0***	***0***
202	5.3	HI	28	4	0
139	12.3	OR	393	72	12
179	7.7	OR	124	16	0
121	15.3	Guam	332	8	0
196	6.2	Guam	114	6	0
144	***11.4***	***FL***	***319***	***11***	***0***
160	***11.2***	***NH***	***392***	***19***	***4***
163	2.6	Marshall Isl.	122	0	0
166	8.4	Oc Stn Papa	233	92	22
197	6.2	Saipan	55	1	0
TOTALS	**397.4**		**8499**	**808**	**76**

4.2 Results of preliminary current analysis

To examine the effects of surface currents and wind on rogue wave development, we performed a preliminary analysis of data from selected buoys (Figure 1) together with modeled ocean surface currents. For time periods of identified rogue wave events at the CDIP buoys #029, 071, 139, and 166, we obtained surface current data from NCEP Climate Forecast System (CFSv2) reanalyses, as noted earlier. Although additional data were processed, the sample analysis results presented here are primarily limited to buoy #029.

Our initial investigation simply looked at mean current direction in comparison to the directions of each spectral component frequency for several times at which rogue waves were detected by specific buoys. An example of these results is provided in Figure 2, which includes sample time series of surface elevation in which a rogue wave was detected at buoy #029, together with a scatter plot of all wave periods in the time series and a panel comparing surface current direction to wave spectral density at each frequency. In this case, the surface currents directly oppose the peak frequency component waves of the spectrum, suggesting that there may have been at least a current-induced Doppler shift in the waves that steepened them and contributed to rogue development.

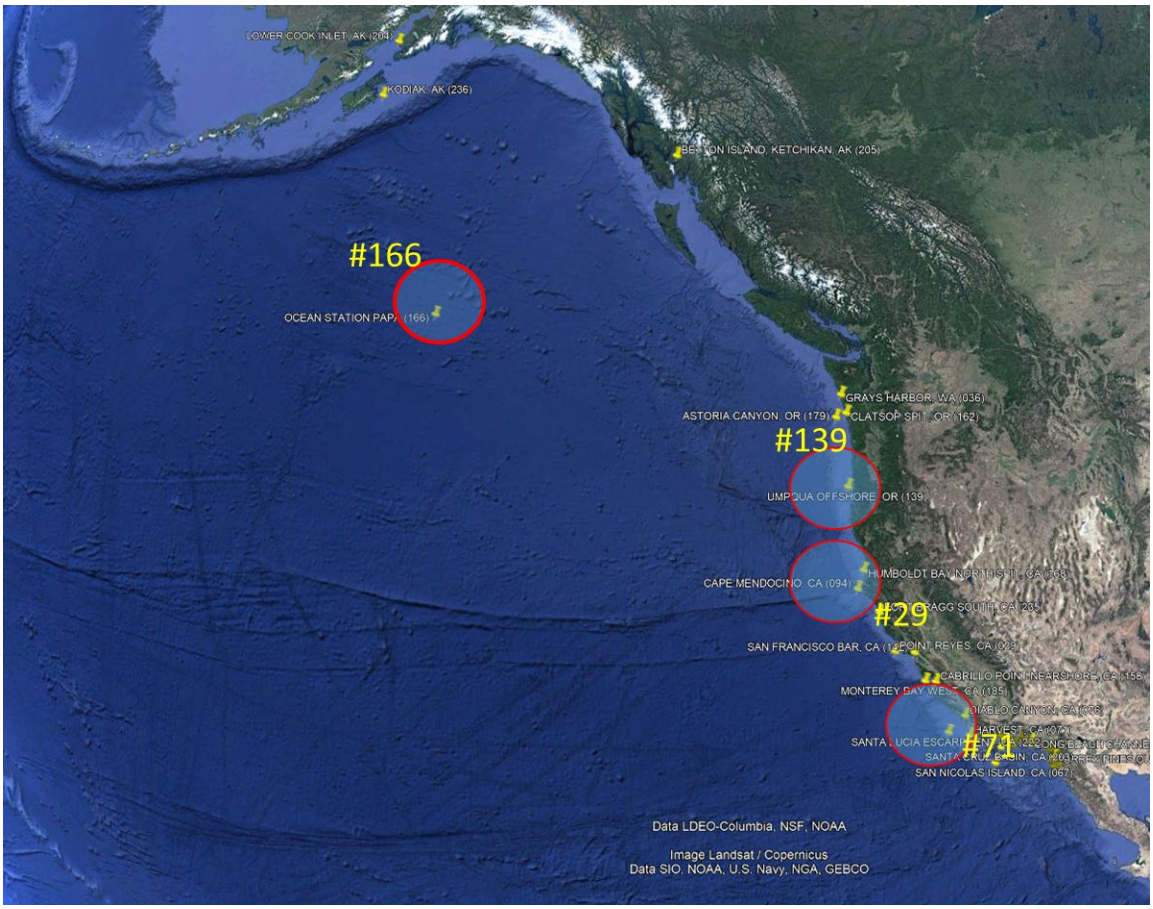

Figure 1. Locations of analyzed buoys (NB: Only selected analysis results – from buoy #029 – are included in this report).

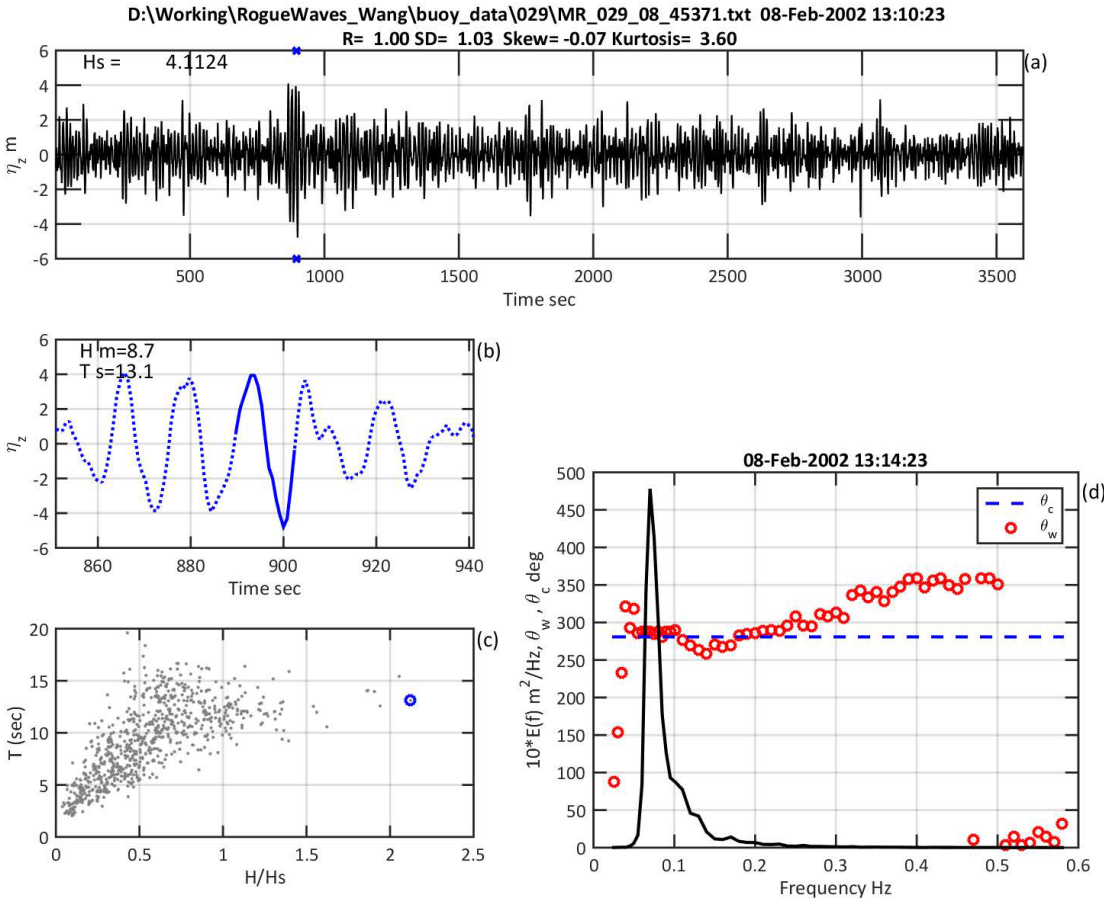

Figure 2. ***Current-only*** analysis results from analysis of rogue wave event at CDIP buoy #29, 08 Feb 2002. Panels show: (a) Original surface elevation time series from buoy. (b) Close up view of 8.7m rogue wave (solid blue line) selected from time series (dashed blue). (c) Scatter plot of wave period (T) vs. normalized wave height (H/H_s) for all waves in the one-hour selection. (d) Wave frequency spectrum (black line), ocean current nautical ("from") direction (θ_c, blue dashed line), and wave Cartesian ("to") direction (θ_w, red circles), plotted versus wave frequency. (*NB: Y-axis on this panel gives units of both* ***10*[spectral density]*** *and directional* ***degrees rel true N***.) Currents are directly opposing the waves for most of the frequencies surrounding the spectral peak.

A follow-up examination determined the direction of the current gradient (θ_g), again for regions surrounding each buoy, using the procedure outlined in Section 3.2. We compared these to wave directions $\theta_w(f)$, particularly the peak spectral direction, for several dozen identified rogue wave events. As noted earlier, results from Manolidis et al. (2019) and others indicate that rogue wave development will be accelerated for cases when waves are propagating into a decreasing current gradient (i.e., either waves are opposed by a current that increases in magnitude as they progress into it, or waves are traveling with a current that is decreasing in magnitude). In this case, such negative current gradient will occur when the value of the cosine term in equation (1) above is negative. This requires the absolute difference between θ_g and $\theta_w(f)$ to be more than 90° but less than 270°, with the greatest spectral modulating effect occurring when the two angles differ by 180°.

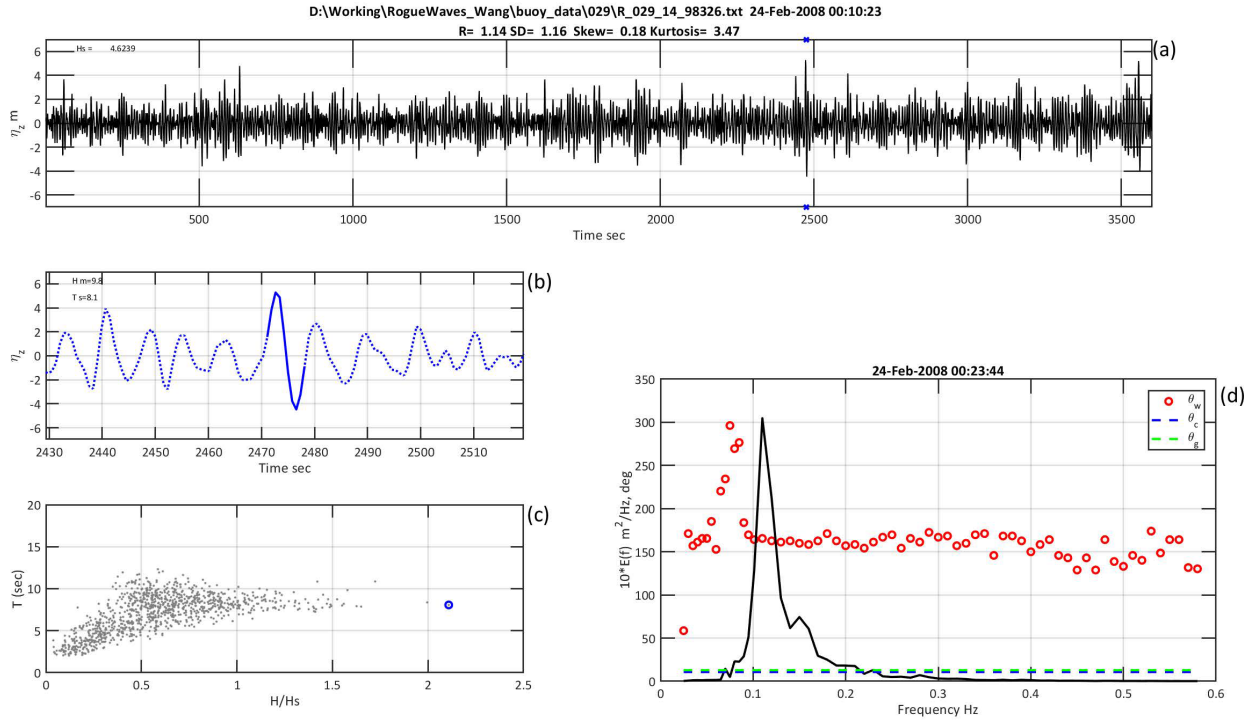

Figure 3. ***Current gradient*** analysis results for rogue event identified at buoy #029, 24 Feb 2008. Format is same as that of Figure 2, except that lower right panel also includes a green dashed line representing the Cartesian ("to") direction computed for the surface current gradient. For the event shown, the wave direction at the spectral peak frequency $\theta_w(f) \approx 170°$, while the current gradient direction $\theta_g \approx 10°$, so that $|\theta_w(f) - \theta_g| \approx 160°$, indicating that the peak waves are propagating into a primarily negative current gradient in this case.

Our results were rather mixed, as can be seen from the sample buoy #029 data in Figure 3 – Figure 7. Each figure shows analysis for an individual rogue wave event identified at the buoy, including surface elevation time series, a scatter plot of wave height and period, and a combined plot of wave spectrum and wave direction versus frequency, with separate lines showing direction of the local current and current gradient (format is very similar to that of Figure 2). The first three figures (Figure 3 – Figure 5) provide support for the theoretical results described in the Introduction. In each case, the difference between the peak wave direction of the rogue wave spectrum (black solid line) and the current gradient direction (green dashed line) is significantly greater than 90° but also less than 270°, indicating that the spectral peak waves are propagating into a negative current gradient (as described in Section 3.2 above), which should contribute to further modulation of waves at those frequencies. However, the latter two figures (Figure 6 – Figure 7) provide sample data that do not match the theory. In each of these figures, the difference between the peak wave direction and the current gradient direction is less than 90°, despite the fact that the measured waves in both cases are clearly rogue waves.

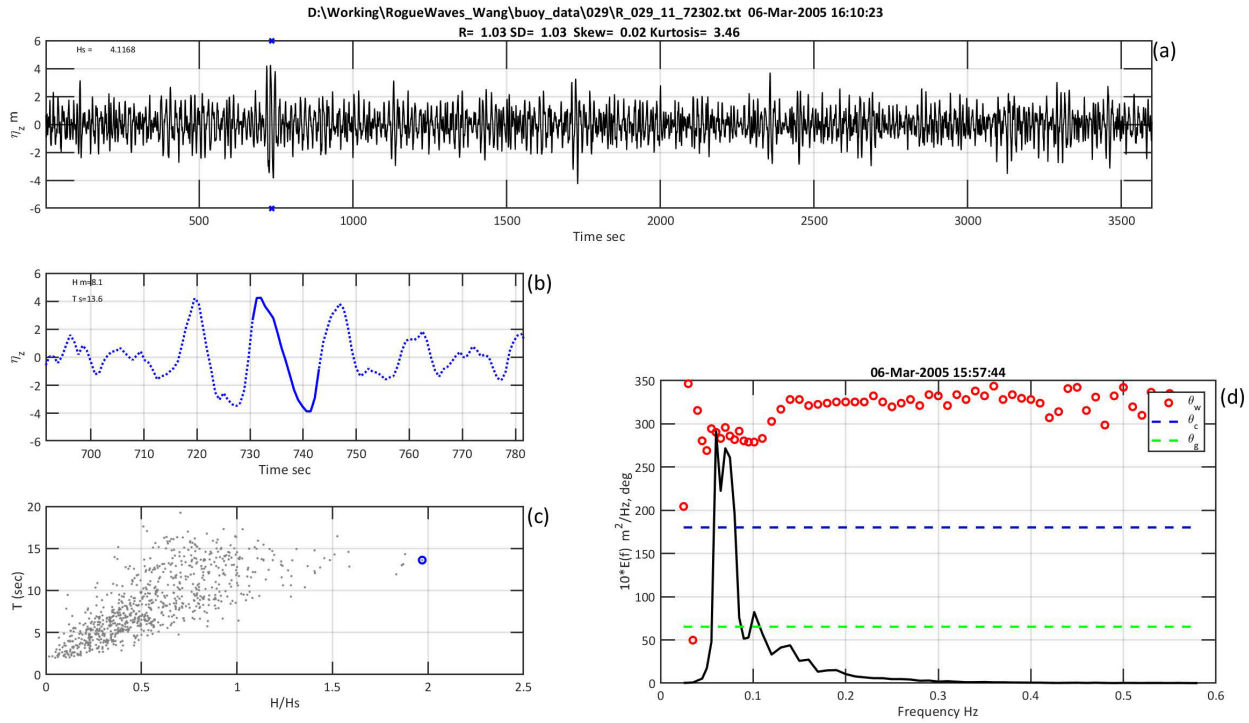

Figure 4. Current gradient analysis results for rogue event identified at buoy #029, 06 Mar 2008. Format is same as that of Figure 3. For the event shown, the wave direction at the spectral peak frequency $\theta_w(f) \approx 300°$, while the current gradient direction $\theta_g \approx 60°$, so that $|\theta_w(f) - \theta_g| \approx 140°$, indicating that the peak waves are again propagating into a primarily negative current gradient in this case.

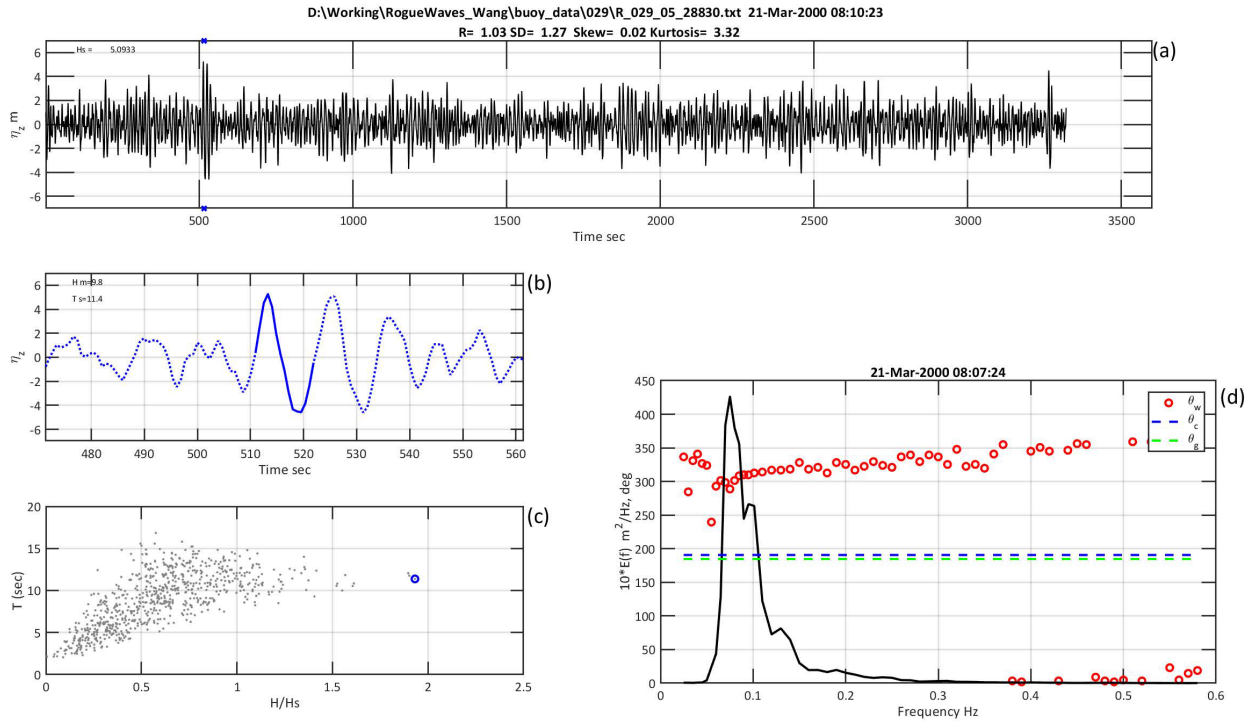

Figure 5. Current gradient analysis results for rogue event identified at buoy #029, 21 Mar 2008. Format is same as that of Figure 3. For the event shown, the wave direction at the spectral peak frequency $\theta_w(f) \approx 300°$, while the current gradient direction $\theta_g \approx 190°$, so that $|\theta_w(f) - \theta_g| \approx 110°$, indicating that the peak waves are propagating into an only weakly negative current gradient in this case.

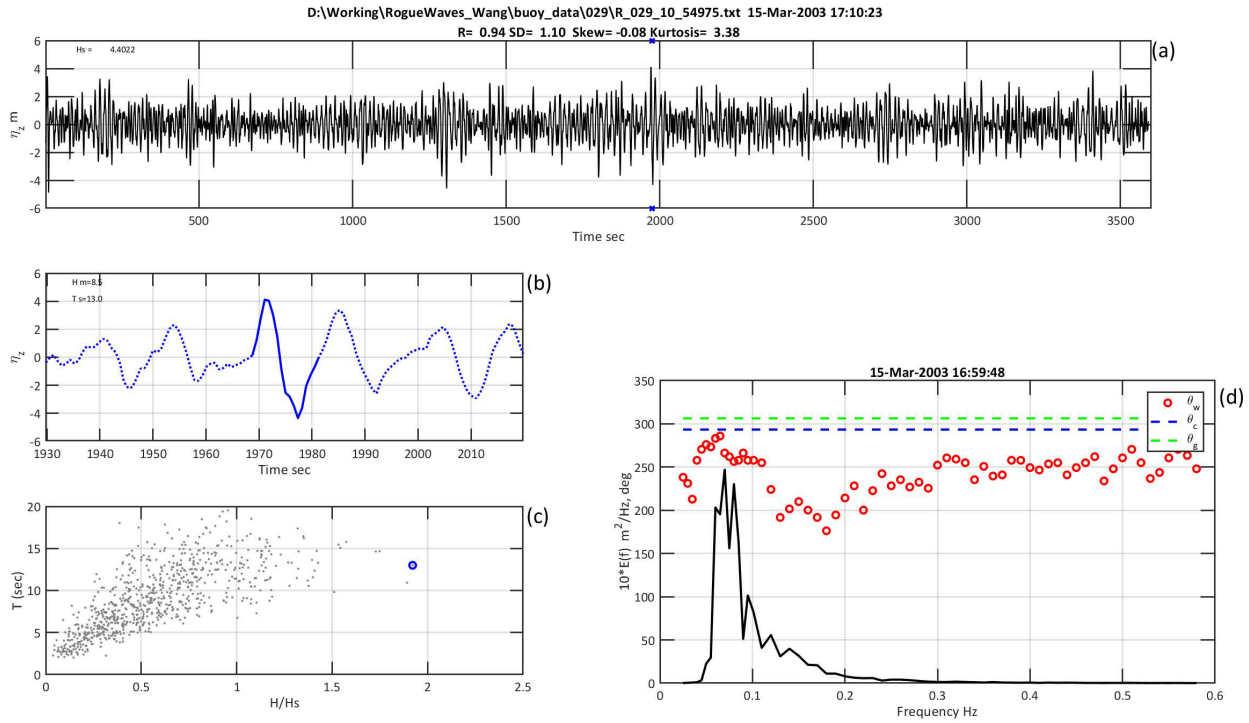

Figure 6. Current gradient analysis results for rogue event identified at buoy #029, 15 Mar 2008. Format is same as that of Figure 3. For the event shown, the wave direction at the spectral peak frequency $\theta_w(f) \approx 260°$, while the current gradient direction $\theta_g \approx 310°$, so that $|\theta_w(f) - \theta_g| \approx 50°$, indicating that the peak waves are propagating into a positive current gradient in this case, contrary to what would be expected for most current-forced rogue wave events.

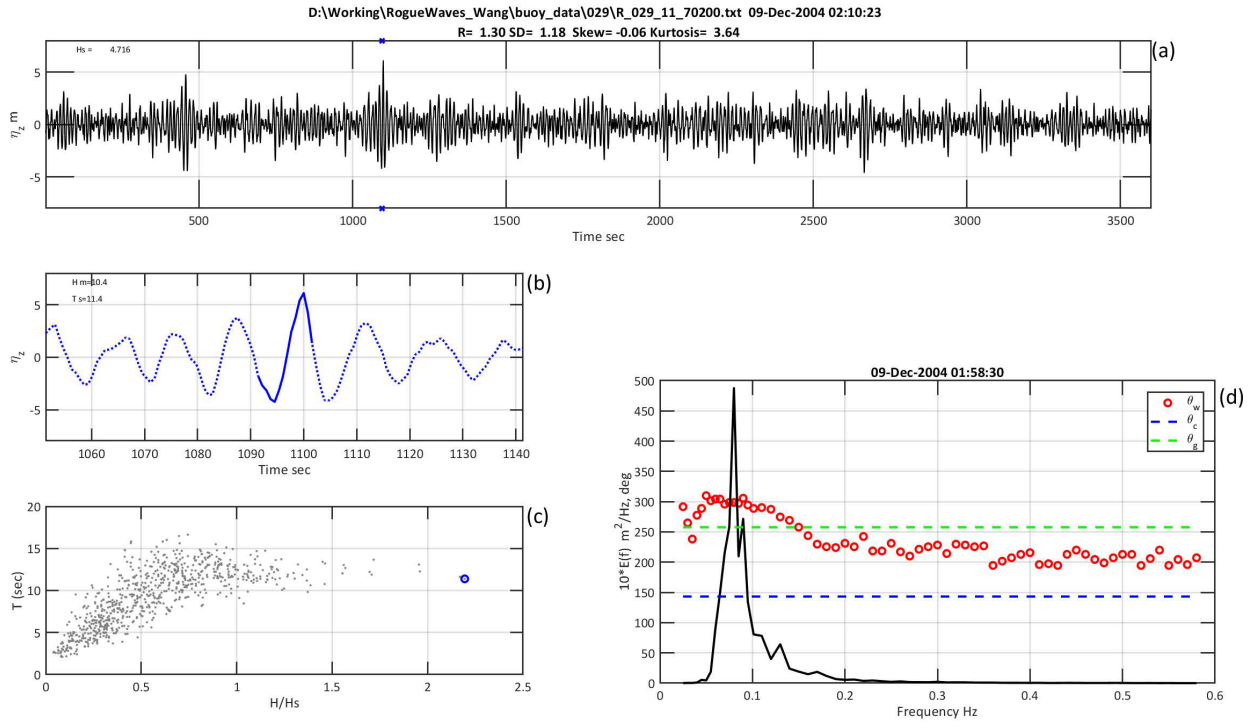

Figure 7. Current gradient analysis results for rogue event identified at buoy #029, 09 Dec 2004. Format is same as that of Figure 3. For the event shown, the wave direction at the spectral peak frequency $\theta_w(f) \approx 300°$, while the current gradient direction $\theta_g \approx 260°$, so that $|\theta_w(f) - \theta_g| \approx 40°$, indicating (as in Figure 6) that the peak waves are propagating into a positive current gradient, contrary to what would be expected for most current-forced rogue wave events.

An additional environmental factor that may contribute to rogue wave development but has not been considered here is the bottom bathymetry. Particularly for very long waves in shallower coastal regions, bathymetric shoaling and refraction effects can add significantly to nonlinear wave growth. The location of at least two of the selected wave buoys, #029 and #071, provide at least limited support for the idea that some measured rogue waves may occasionally be bathymetry-forced at these sites (Figure 8).

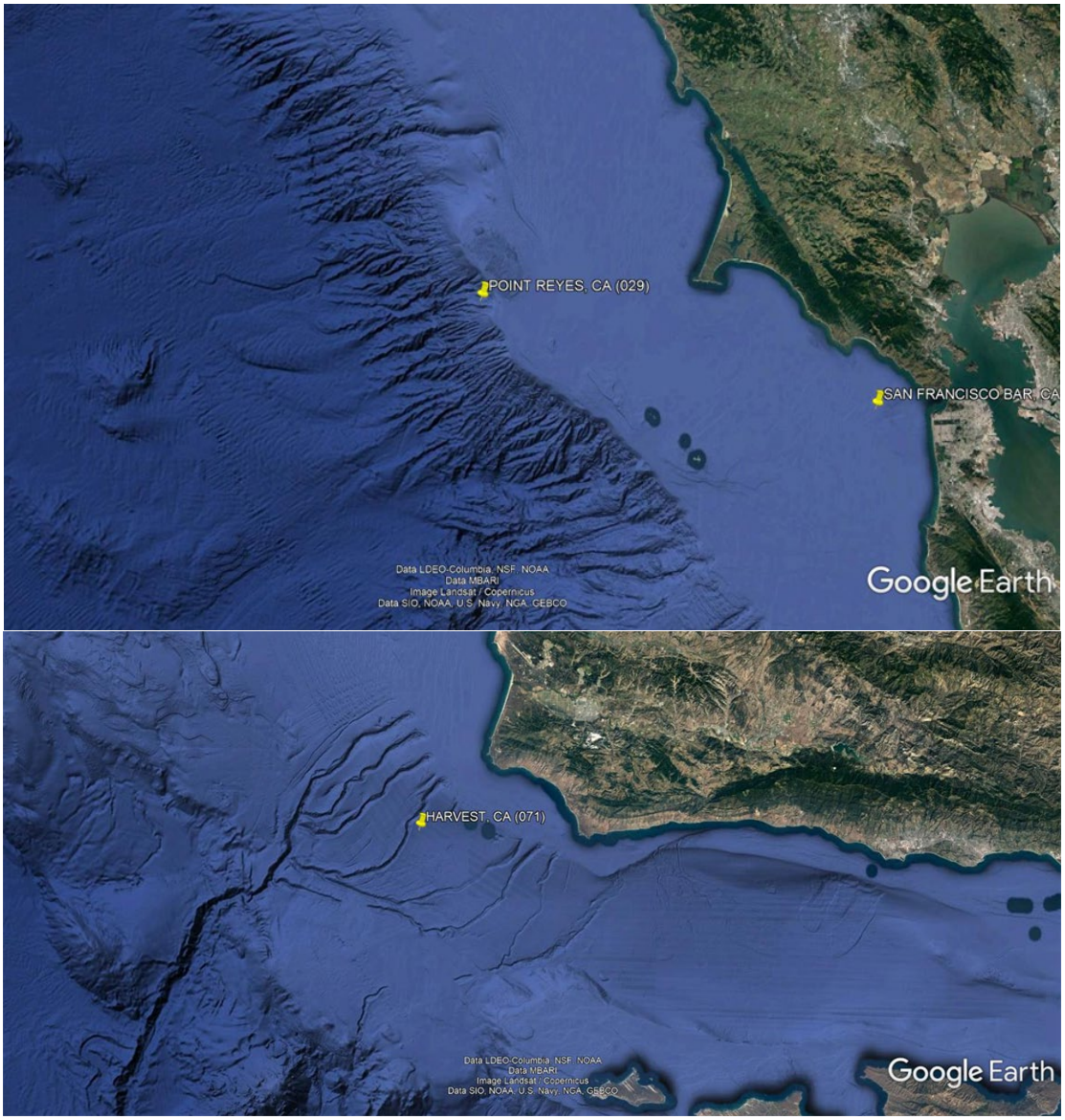

Figure 8. Location of buoys #029 (top) and #071 (bottom) over bathymetry. Buoy is near shelf edge in each case.

5 CONCLUSIONS AND FUTURE WORK

In this report, we have summarized an extensive analysis of nearly 400 years of buoy surface elevation time series, in which we have identified and confirmed roughly 8500 rogue wave events. Our results add to the evidence that these anomalously large waves may be found anywhere in the open-water global ocean, with many such events occurring on any given day.

Of course, rogue waves that are only a few meters in height do not generally pose a threat to most ocean-going vessels, even though they exceed twice the local significant wave height. The criteria for a "dangerous" rogue wave are highly dependent on the specific vessel that encounters one. In our analysis, we have identified over 800 rogue events involving waves over 6m high, and nearly 80 events with waves exceeding 10m. While 80 extreme rogue waves over an almost 400-year period may seem relatively small (i.e., one big wave every 5 years), it should be noted that this tally only includes 34 specific locations. If we assume that each buoy location represents a surface area of $10km^2$, these buoys cumulatively monitor an area of $340km^2$, which is approximately one millionth (i.e., 10^{-6}) of the surface of the global ocean (excluding the Arctic Ocean). This reasoning suggests that the global ocean will see roughly one million big waves every 5 years, or about ***500*** rogue waves exceeding 10m each day.

Assuming that its "region of vulnerability" is $\pm$250m to either side, a container ship traveling at average speed of 25km/hr will cover a "vulnerable area" of about $300km^2$ each day. For a one-week trip, our data suggest that the container ship will have approximately a 1 in 250 chance of encountering a 10m or greater rogue wave during its passage. For the roughly 6000 container ships that are active at any given moment in the world's oceans, this result implies that 20 or more will see a large rogue wave for each week they are at sea.

The effect of ocean current gradients on nonlinear modulation of wave spectra has yet to be confirmed in the field. Results from our limited analysis are decidedly mixed, as illustrated in Section 4.2 above. It should be noted that the above analysis relies on surface current data with a grid spacing of 0.5 degree, provided at a time step of 6 hours. In addition to this limited resolution, there is also some question as to the accuracy of surface current reanalysis data in comparison to actual ocean currents at the small horizontal length scales most relevant to rogue wave events. A thorough and complete field-based evaluation of the effect of current gradients on rogue waves will require much more careful measurement of both waves and currents over a domain of at least O(10 km^2) with grid spacing of O(1-10 m). This sort of dataset might be acquired with ship- or platform-based, high-resolution x-band radar systems in a dedicated deployment over at least several weeks.

The primary goal of these and other rogue wave investigations at NRL has been to develop an efficient and effective warning system to provide Navy and civilian vessels with actionable estimates of rogue wave threat in a full range of oceanic environments. To this end, a prototype rogue threat index (RTI) estimation utility has been developed for the WAVEWATCH III model (see Orzech et al., 2019). This utility estimates the threat of rogue development based on an evaluation of four contributing environmental factors (modulation instability of the wave spectrum, surface current gradients, wave directional distribution, and wind effects). In FY20-22, we plan to fully test, calibrate, and validate this warning system, ultimately transitioning it to the operational WAVEWATCH III. These datasets will be heavily utilized in the calibration and validation, which will modify weighting in the rogue threat computation to maximize the correlation of larger estimated RTI with the "positive" signals of confirmed rogue events from the buoys.

6 REFERENCES

Babanin, A., and W.E. Rogers, 2014: Generation and limiters of rogue waves. *Int. J. Oc. Clim. Sys*. **5(2)**, 39-49.

Datawell BV, 2009: Datawell waverider reference manual (WR-SG, DWR-MkIII, DWR-G), Harlem, Netherlands, 123pp. https://cdip.ucsd.edu/documents/index/gauge_docs/mk3.pdf.

Janssen, P.A.E.M., 2003: Nonlinear four-wave interactions and freak waves. *J. Phys. Oceanogr*., **33**, 863–88.

Manolidis, M., M. Orzech, and J. Simeonov, 2019: Rogue wave formation in adverse current gradients, *J. Mar. Sci. & Engrg*.. **7(26)**, doi:10.3390/jmse7020026.

Onorato, M., D. Proment, and A. Toffoli, 2011: Triggering rogue waves in opposing currents. *Phys. Rev. Lett*., **107**, 184502.

Onorato, M., et al., 2009: Statistical properties of mechanically generated surface gravity waves: A laboratory experiment in a 3D wave basin, *J. Fluid Mech*., **627**, 235–257.

Orzech, M., J. Simeonov, and M. Manolidis, 2019: Development and testing of a rogue wave threat estimator for WAVEWATCH III®, *NRL Memorandum Report*, submitted Sep. 2019.

Saha, S., et al., 2010: The NCEP climate forecast system reanalysis, Bull. Amer. Meteor. Soc., **91**, 1015–1058, doi:10.1175/2010BAMS3001.1.

Waseda, T., T. Kinoshita, and H. Tamura, 2009: Evolution of a random directional wave and freak wave occurrence. *J. Phys. Oceanog*., **39**, 621–639.

WAVEWATCH III® Development Group (WW3DG), 2019: User manual and system documentation of WAVEWATCH III® version 6.07. Tech. Note 333, NOAA/NWS/NCEP/MMAB, College Park, MD, USA, 320 pp. + Appendices.